

# Unintegrated gluon distributions in $D^{*\pm}$ and dijet associated photoproduction at HERA

A.V. Lipatov<sup>a</sup>, N.P. Zotov

D.V. Skobeltsyn Institute of Nuclear Physics, M.V. Lomonosov Moscow State University, 119992 Moscow, Russia

Received: 12 December 2005 / Revised version: 13 February 2006 /  
Published online: 14 July 2006 – © Springer-Verlag / Società Italiana di Fisica 2006

**Abstract.** We consider the photoproduction of  $D^{*\pm}$  mesons associated with two hadron jets at HERA collider in the framework of the  $k_T$ -factorization approach. The unintegrated gluon densities in a proton are obtained from the full CCFM, from unified BFKL-DGLAP evolution equations as well as from the Kimber–Martin–Ryskin prescription. Resolved photon contributions are reproduced by the initial-state gluon radiation. We investigate different production rates and make a comparison with the recent experimental data taken by the ZEUS collaboration. Special attention is given to the specific dijet correlations which can provide unique information about non-collinear gluon evolution dynamics.

## 1 Introduction

The production of heavy flavor (charm and bottom) in electron–proton collisions at HERA is a subject of intensive studies from both the theoretical and experimental point of view [1–5]. From the theoretical side, heavy quarks in  $ep$  interactions can be produced via direct (photon–gluon fusion) and resolved production mechanisms. In resolved events, the photon emitted by the electron fluctuates into a hadronic state, and a gluon and/or a quark of this hadronic fluctuation takes part in the hard interactions. It is expected that resolved photon processes contribute significantly in the photoproduction region, in which the photon is quasi-real ( $Q^2 \sim 0$ ) and to be suppressed towards higher  $Q^2$ . Therefore charm and bottom photoproduction cross sections are sensitive to the parton (quark and gluon) content of the proton as well as of the photon.

Usually quark and gluon densities are described by the Dokshitzer–Gribov–Lipatov–Altarelli–Parizi (DGLAP) evolution equation [6] where large logarithmic terms proportional to  $\ln \mu^2$  are taken into account only. The cross sections can be rewritten in terms of process-dependent hard matrix elements convoluted with quark or gluon density functions. In this way the dominant contributions come from diagrams where parton emissions in the initial state are strongly ordered in virtuality. This is called collinear factorization, as the strong ordering means that the virtuality of the parton entering the hard scattering matrix elements can be neglected compared to the large scale  $\mu$ . However, at high energies this hard scale is large compared to the  $\Lambda_{\text{QCD}}$  parameter, but on the other hand  $\mu$  is much smaller than the total energy  $\sqrt{s}$  (around 300 GeV for the

HERA collider). Therefore in such a case it was expected that the DGLAP evolution, which is only valid at large  $\mu^2$ , should break down. The situation is classified as “semi-hard” [7–10]. It is believed that at asymptotically large energies (or small  $x \sim \mu^2/s$ ) the theoretically correct description is given by the Balitsky–Fadin–Kuraev–Lipatov (BFKL) evolution equation [11], because here large terms proportional to  $\ln 1/x$  are taken into account. Just as for DGLAP, in this way it is possible to factorize an observable into a convolution of process-dependent hard matrix elements with universal gluon distributions. But as the virtualities (and transverse momenta) of the propagating gluons are no longer ordered, the matrix elements have to be taken off-shell and the convolution made also over transverse momentum  $\mathbf{k}_T$  with the unintegrated (i.e.  $k_T$ -dependent) gluon distribution. This generalized factorization is called  $k_T$ -factorization [7–10].

The unintegrated gluon distribution is subject of intensive studies at present [12, 13]. Various approaches to investigate this quantity have been proposed. Thus, there is the unified BFKL-DGLAP equation [14] which incorporates both the resummed leading  $\ln 1/x$  and the resummed leading  $\ln \mu^2$  contributions. Another approach, valid for both small and large  $x$  also, has been developed by Ciafaloni, Catani, Fiorani and Marchesini and is known as the CCFM model [15]. It introduces angular ordering of emissions to correctly treat gluon coherence effects. In the limit of asymptotic energies, it is almost equivalent to BFKL [16–18], but also similar to the DGLAP evolution for large  $x$  and high  $\mu^2$ . The resulting unintegrated gluon distribution depends on two scales; the additional scale  $\bar{q}$  is a variable related to the maximum angle allowed in the emission and plays the role of the evolution scale  $\mu$  in the collinear parton densities. Also it is possible to obtain the two-scale involved unintegrated gluon distributions from

<sup>a</sup> e-mail: lipatov@theory.sinp.msu.ru

the conventional ones using the Kimber–Martin–Ryskin (KMR) prescription [19]. In this way the  $\mu$  dependence in the unintegrated gluon distribution enters only in last step of the evolution, and single-scale evolution equations can be used up to this step. The unintegrated gluon densities have the advantage that, in particular, they take into account the true kinematics of the process under consideration even at leading order and are more suitable for less inclusive processes.

Recently the ZEUS collaboration has presented new experimental data [2, 3] on the charm production in electron–proton collisions at HERA, namely the results of measurements of the  $D^{*\pm}$  meson production rates both inclusive and associated with one or two hadronic jets. Concerning the theoretical treatment of charm photoproduction in the framework of standard (collinear) QCD, two types of NLO calculations are available for comparison with the experimental data. The massive charm approach [20] assumes that light quarks are the only active flavors in the structure functions of the proton and photon, so that charm (and beauty) are produced only in the hard process. In the massless scheme [21, 22] charm and beauty are treated as additional active flavors (massless partons). These two approaches are applicable in different regions: for  $p_T^2 \simeq m_c^2$  and  $p_T^2 \geq m_c^2$  respectively. The massless charm calculations take into account charm-excitation processes and thus predict a larger resolved component in comparison with the massive calculations. The photoproduction of a  $D^*$  meson in association with a hadron jet was described recently in the next-to-leading order of QCD using non-perturbative fragmentation functions [23]. It was shown that the transverse momentum and rapidity distributions measured at HERA [3] well agree with theoretical predictions. These comparisons also illustrate the significance of the charm component in the resolved photon. Unfortunately the dijet angular distributions [2] and correlations [3] in charm photoproduction, which give a clearer test for the manifestation of the relative role of the direct and resolved photon contributions, were not described in this approach. The NLO QCD predictions in the massive scheme [20] are in general agreement with the data although differences have been isolated in regions where contributions from higher orders are expected to be significant [3].

In the present paper we will consider the associated  $D^*$  and dijet photoproduction using the  $k_T$ -factorization approach. There are several motivations for such a study. First of all, in the framework of the  $k_T$ -factorization approach it was demonstrated [24, 25] that resolved photon-like contributions are effectively simulated by gluon evolution in the initial state and are described by the unintegrated gluon distribution in the proton. The fraction  $x_\gamma^{\text{obs}}$  of the photon momentum which participates in the dijet production has been measured in [1–3]. This quantity is sensitive to the relative contributions of resolved and direct processes in collinear fixed-order QCD calculations [1]. In leading order (LO), direct photon events at the parton level have  $x_\gamma^{\text{obs}} = 1$ , while resolved photon events populate low values of  $x_\gamma^{\text{obs}}$ . The same situation is observed in next-to-leading (NLO) calculations, because in the three par-

ton final state any of these partons are allowed to take any kinematically accessible value. In the  $k_T$ -factorization formalism the hardest transverse momentum parton emission can be anywhere in the evolution chain and does not need to be closest to the photon as required by the strong  $\mu^2$  ordering in DGLAP. Thus, if the two hardest jets are produced by the  $c\bar{c}$  pair, then  $x_\gamma^{\text{obs}}$  is close to unity, but if a gluon from the initial cascade and one of the final charmed quarks form the two hardest transverse momentum jets, then  $x_\gamma^{\text{obs}} < 1$ .

Another interesting quantity is the measured distribution of the outgoing jets with a  $D^*$  in the final state on the angle  $\theta^*$  between the jet–jet axis and the proton beam direction in the dijet rest frame. This quantity is sensitive to the spin of the propagator in the hard subprocess [2]. In direct photon processes  $\gamma g \rightarrow c\bar{c}$  the propagator in the LO QCD diagrams is a quark, and the differential cross section increases slowly towards high  $|\cos\theta^*|$  values. In resolved processes, the gluon propagator is allowed at LO and dominates over the quark propagator due to the stronger gluon–gluon coupling compared to the quark–gluon coupling. If most of the resolved photon charm dijet events are produced as a result of charm from the photon, a gluon-exchange contribution in the  $cg \rightarrow cg$  subprocess should dominate. This results in a steep rise of the cross section towards high  $|\cos\theta^*|$  values. If one of the jets is explicitly tagged as a charm jet, the sign of  $\cos\theta^*$  can be defined [2]. In the  $k_T$ -factorization approach the  $\cos\theta^*$  distribution is determined only by the photon–gluon fusion off-shell matrix element which covers both scattering process. This is because there is no restriction on the transverse momenta along the evolution cascade, as it was already mentioned above.

Third, previously unmeasured correlations between the two jets, namely the difference in azimuthal angle  $\Delta\phi$  and the transverse momentum of the dijet system  $p_T$  have been presented recently [3]. These quantities are particularly sensitive to high-order correction effects. So, in the collinear LO approximation, the two jets are produced back-to-back with  $\Delta\phi = \pi$  and  $p_T = 0$ . Large deviations from these values may come from higher-order QCD effects. Taking into account the non-vanishing initial parton transverse momenta leads to the violation of this back-to-back kinematics in the  $k_T$ -factorization approach even at leading order. It has been shown [26] that theoretical and experimental studying of the  $\Delta\phi$  distributions is a direct probe of the non-collinear parton evolution.

In previous studies [24, 25] the  $k_T$ -factorization approach has already been applied to the calculation of the  $x_\gamma^{\text{obs}}$  and  $|\cos\theta^*|$  distributions of the charm and dijet photoproduction at HERA. A steep rise in the cross section with increasing  $|\cos\theta^*|$  for resolved photon-like events compared to the direct photon-like events through the initial-state gluon cascade [25] was observed. It was claimed that this effect in the  $k_T$ -factorization approach can be interpreted as “charm-excitation” processes. However, the comparisons with the experimental data on the  $|\cos\theta^*|$  distributions were done [27] only in the framework of the Monte Carlo generator CASCADE [28]. The azimuthal correlations between the transverse momenta of

the produced jets and the  $p_T$  distributions have not been investigated up to this time.

In this paper we study the associated  $D^*$  and dijet photoproduction at HERA in more detail. We calculate a number of different production rates and compare our theoretical results with the recent ZEUS data [1–3]. Special attention will be given to the specific dijet correlations which are sensitive to the transverse momentum of the partons incoming to the hard scattering process and therefore sensitive to the details of the unintegrated gluon density, as it was mentioned above. We will test the unintegrated gluon distributions which are obtained from the full CCFM, unified BFKL-DGLAP evolution equations, and from the conventional (DGLAP-based) gluon densities. In the last case we use the KMR prescription.

The outline of our paper is as follows. In Sect. 2 we recall the basic formulas of the  $k_T$ -factorization formalism with a brief review of the calculation steps. In Sect. 3 we present the numerical results of our calculations and a discussion. Finally, in Sect. 4, we give some conclusions.

## 2 Basic formulas

Let  $p_e$  and  $p_p$  be the four-momenta of the initial electron and proton, and  $p_c$  and  $p_{\bar{c}}$  the four-momenta of the produced charmed quarks. The charm photoproduction cross section in the  $k_T$ -factorization approach can be written as

$$\begin{aligned} d\sigma(\gamma p \rightarrow c\bar{c} + X) \\ = \int \frac{dx}{x} \mathcal{A}(x, \mathbf{k}_T^2, \mu^2) d\mathbf{k}_T^2 \frac{d\phi}{2\pi} d\hat{\sigma}(\gamma g^* \rightarrow c\bar{c}), \end{aligned} \quad (1)$$

where  $\mathcal{A}(x, \mathbf{k}_T^2, \mu^2)$  is the unintegrated gluon distribution,  $\hat{\sigma}(\gamma g^* \rightarrow c\bar{c})$  is the charm production cross section via an off-shell gluon having a fraction  $x$  of the initial proton longitudinal momentum, non-zero transverse momentum is  $\mathbf{k}_T$  ( $\mathbf{k}_T^2 = -k_T^2 \neq 0$ ) and we have the azimuthal angle  $\phi$ . The expression (1) can be easily rewritten as

$$\begin{aligned} \frac{d\sigma(\gamma p \rightarrow c\bar{c} + X)}{dy_c d\mathbf{p}_{cT}^2} \\ = \int \frac{1}{16\pi(xs)^2(1-\alpha)} \mathcal{A}(x, \mathbf{k}_T^2, \mu^2) |\bar{\mathcal{M}}|^2(\gamma g^* \rightarrow c\bar{c}) \\ \times d\mathbf{k}_T^2 \frac{d\phi}{2\pi} \frac{d\phi_c}{2\pi}, \end{aligned} \quad (2)$$

where  $|\bar{\mathcal{M}}|^2(\gamma g^* \rightarrow c\bar{c})$  is the squared off-shell matrix element,  $s = (p_\gamma + p_p)^2$  is the total center-of-mass frame energy,  $y_c$  and  $\phi_c$  are the rapidity and the azimuthal angle of the produced charmed quark having mass  $m_c$ ,  $\alpha = m_{cT} \exp(y_c) / \sqrt{s}$  and  $m_{cT}^2 = m_c^2 + \mathbf{p}_{cT}^2$ . The analytic expression for the  $|\bar{\mathcal{M}}|^2(\gamma g^* \rightarrow c\bar{c})$  was obtained in our previous paper [29]. We would like to note that if we average (2) over  $\mathbf{k}_T$  and take the limit  $\mathbf{k}_T^2 \rightarrow 0$ , then we obtain the usual formula for the charm production in LO perturbative QCD.

The available experimental data [1–3] taken by the ZEUS collaboration refer to the charm photoproduction

in  $ep$  collisions, where the electron is scattered at a small angle, and the mediating photon is almost real ( $Q^2 \sim 0$ ). Therefore  $\gamma p$  cross section (2) needs to be weighted with the photon flux in the electron:

$$d\sigma(ep \rightarrow c\bar{c} + X) = \int f_{\gamma/e}(y) dy d\sigma(\gamma p \rightarrow c\bar{c} + X), \quad (3)$$

where  $y$  is the fraction of the initial electron energy taken by the photon in the laboratory frame, and we use the Weizacker–Williams approximation for the bremsstrahlung photon distribution from an electron:

$$\begin{aligned} f_{\gamma/e}(y) \\ = \frac{\alpha_{em}}{2\pi} \left( \frac{1+(1-y)^2}{y} \ln \frac{Q_{\max}^2}{Q_{\min}^2} + 2m_e^2 y \left( \frac{1}{Q_{\max}^2} - \frac{1}{Q_{\min}^2} \right) \right). \end{aligned} \quad (4)$$

Here  $\alpha_{em}$  is Sommerfeld’s fine structure constant,  $m_e$  is the electron mass,  $Q_{\min}^2 = m_e^2 y^2 / (1-y)$  and  $Q_{\max}^2 = 1 \text{ GeV}^2$ , which is a typical value for the recent photoproduction measurements at the HERA collider.

The basic photon–gluon fusion subprocess under consideration ( $\gamma g^* \rightarrow c\bar{c}$ ) gives rise to two high-energy charmed quarks, which can further evolve into hadron jets. In our calculations the produced quarks (with their known kinematical parameters) were taken to play the role of the final jets. These two quarks are accompanied by a number of gluons radiated in the course of the gluon evolution. As it has been noted in [24], on the average the gluon transverse momentum decreases from the hard interaction block towards the proton. As an approximation, we assume that the gluon emitted in the last evolution step and having the four-momentum  $k'$  compensates the whole transverse momentum of the gluon participating in the hard subprocess, i.e.  $\mathbf{k}'_T \simeq -\mathbf{k}_T$ . All the other emitted gluons are collected in the proton remnant, which is assumed to carry only a negligible transverse momentum compared to  $\mathbf{k}'_T$ . This gluon gives rise to a final hadron jet with  $E_T^{\text{jet}} = |\mathbf{k}'_T|$  in addition to the jet produced in the hard subprocess. From these three hadron jets we choose the two ones carrying the largest transverse energies, and then compute the charm and associated dijet production rates.

As it was noted already, the variable  $x_\gamma^{\text{obs}}$  is often used in the analysis of the recent experimental data. This variable, which is the fraction of the photon momentum contributing to the production of the two jets with the highest transverse energies  $E_T^{\text{jet}}$ , experimentally is defined as

$$x_\gamma^{\text{obs}} = \frac{E_T^{\text{jet}1} e^{-\eta^{\text{jet}1}} + E_T^{\text{jet}2} e^{-\eta^{\text{jet}2}}}{2yE_e}, \quad (5)$$

where  $yE_e$  is the initial photon energy and the  $\eta^{\text{jet}i}$  are the pseudo-rapidities of these hardest jets. The pseudo-rapidities  $\eta^{\text{jet}i}$  are defined as  $\eta^{\text{jet}i} = -\ln \tan(\theta^{\text{jet}i}/2)$ , where  $\theta^{\text{jet}i}$  are the polar angles of the jets with respect to the proton beam. The selection of  $x_\gamma^{\text{obs}} > 0.75$  and  $x_\gamma^{\text{obs}} < 0.75$  yields samples enriched in direct and resolved

photon processes, respectively. The complementary variable is

$$x_p^{\text{obs}} = \frac{E_T^{\text{jet}_1} e^{\eta^{\text{jet}_1}} + E_T^{\text{jet}_2} e^{\eta^{\text{jet}_2}}}{2E_p}, \quad (6)$$

which is the fraction of the proton's momentum contributing to the production of the two jets. Other dijet variables such as their scattering angle  $\theta^*$  and invariant mass  $M$  are defined as

$$\cos \theta^* = \tanh \left( \frac{\eta^{\text{jet}_1} - \eta^{\text{jet}_2}}{2} \right), \quad (7)$$

$$M = \sqrt{2E_T^{\text{jet}_1} E_T^{\text{jet}_2} [\cosh(\eta^{\text{jet}_1} - \eta^{\text{jet}_2}) - \cos(\phi^{\text{jet}_1} - \phi^{\text{jet}_2})]}, \quad (8)$$

where the  $\phi^{\text{jet}_i}$  are the azimuthal angles of the corresponding jets.

The multidimensional integration in (2) and (3) has been performed by means of the Monte Carlo technique, using the routine VEGAS [30]. The full C++ code is available from the authors on request<sup>1</sup>.

### 3 Numerical results

We now are in a position to present our numerical results. First we describe our theoretical input and the kinematical conditions. There are several parameters which determined the normalization factor of the cross section under consideration: the charmed quark mass  $m_c$ , the factorization and normalization scales  $\mu_F$  and  $\mu_R$ , the charm fragmentation function and the unintegrated gluon distribution in a proton  $\mathcal{A}(x, \mathbf{k}_T^2, \mu^2)$ . In our calculations we convert the charmed quark into a  $D^*$  meson using the Peterson fragmentation function [31] with  $\epsilon_c = 0.035$  [32]. The branching  $c \rightarrow D^*$  was set to the value measured [33] by the OPAL collaboration:  $f(c \rightarrow D^*) = 0.235$ .

In the further numerical analysis we have tried three different sets of the unintegrated gluon densities in a proton, namely J2003 (set 1) [34], KMS [14] and KMR [19], which are frequently discussed in the literature now<sup>2</sup>. The J2003 density has been obtained from the numerical solution of the full CCFM equation. The input parameters were fitted [34] to describe the proton structure function  $F_2(x, Q^2)$ . The J2003 (set 1) gluon distribution contains only singular terms in the CCFM splitting function  $P_{\text{gg}}(z)$ <sup>3</sup>. This gluon density has been applied, in particular, in the analysis of the forward jet production at HERA, of charm and bottom production at Tevatron [32], and charm and  $J/\psi$  production at LEP2 energies [27]. Another set (KMS) is obtained [14] from a unified BFKL-DGLAP description of the  $F_2(x, Q^2)$  data and includes the so-called consistency constraint [35]. The consistency constraint in-

roduces a large correction to the LO BFKL equation. It was argued [36] that about 70% of the full next-to-leading (NLO) corrections to the BFKL exponent  $\Delta$  are effectively included in this constraint. The last unintegrated gluon distribution used here (the so-called KMR distribution) is the one which was originally proposed in [19]. The KMR approach is the formalism to construct the unintegrated gluon distribution from the known conventional parton densities  $xa(x, \mu^2)$ , where  $a = g$  or  $a = q$ . It accounts for the angular ordering (which comes from the coherence effects in gluon emission) as well as the main part of the collinear higher-order QCD corrections. The KMR-constructed parton densities were used, in particular, to describe the heavy quark and  $J/\psi$  meson production in  $\gamma\gamma$  collisions at LEP2 [29, 37] and prompt photon in photo- and hadroproduction at HERA and Tevatron [38, 39].

The most significant theoretical uncertainties come also from the choice of the factorization and renormalization scales. The first of them is related to the evolution of the gluon distributions  $\mathcal{A}(x, \mathbf{k}_T^2, \mu_F^2)$ , the other one is responsible for the strong coupling constant  $\alpha_s(\mu_R^2)$ . As it often done [20] for charm production, we choose the renormalization and factorization scales to be equal:  $\mu_R = \mu_F = \mu = \sqrt{m_c^2 + \langle \mathbf{p}_T^2 \rangle}$ , where  $\langle \mathbf{p}_T^2 \rangle$  was set to the average  $\mathbf{p}_T^2$  of the charm quark and antiquark<sup>4</sup>. In the present paper we concentrate mostly on the non-collinear gluon evolution in the proton and do not study the scale dependence of our results. For completeness, the charm mass was set to  $m_c = 1.4$  GeV and we use LO formula for the coupling constant  $\alpha_s(\mu^2)$  with  $n_f = 4$  active quark flavors and  $\Lambda_{\text{QCD}} = 200$  MeV, so that  $\alpha_s(M_Z^2) = 0.1232$ .

The recent experimental data [1–3] for the associated  $D^*$  and dijet photoproduction at HERA come from ZEUS collaboration. The data [1] refer to the kinematical region<sup>5</sup> defined by  $130 < W < 280$  GeV,  $Q^2 < 1$  GeV<sup>2</sup> and given for jets with  $|\eta^{\text{jet}}| < 2.4$ ,  $E_T^{\text{jet}_1} > 7$  GeV,  $E_T^{\text{jet}_2} > 6$  GeV and at least one  $D^*$  in the range  $p_T^{D^*} > 3$  GeV,  $-1.5 < \eta^{D^*} < 1.5$ . Results are also presented for the region  $E_T^{\text{jet}_1} > 6$  GeV,  $E_T^{\text{jet}_2} > 5$  GeV. The data [2] have been obtained in the kinematic range  $130 < W < 280$  GeV,  $Q^2 < 1$  GeV<sup>2</sup>,  $p_T^{D^*} > 3$  GeV,  $-1.5 < \eta^{D^*} < 1.5$ ,  $E_T^{\text{jet}} > 5$  GeV and  $|\eta^{\text{jet}}| < 2.4$ . The cuts on the dijet invariant mass  $M > 18$  GeV and on the average jet pseudorapidity  $|\bar{\eta}^{\text{jet}}| < 0.7$  were applied, where  $\bar{\eta}^{\text{jet}}$  is defined as  $\bar{\eta}^{\text{jet}} = (\eta^{\text{jet}_1} + \eta^{\text{jet}_2})/2$ . The more recent data [3] refer to the kinematical region defined by  $E_T^{\text{jet}_1} > 7$  GeV,  $E_T^{\text{jet}_2} > 6$  GeV and  $-1.5 < \eta^{\text{jet}} < 2.4$ . The  $Q^2$ ,  $W$ ,  $p_T^{D^*}$  and  $\eta^{D^*}$  requirements are the same as in the previous measurements.

#### 3.1 The distributions on $x_\gamma^{\text{obs}}$ and $x_p^{\text{obs}}$

In Figs. 1–5 we confront the  $x_\gamma^{\text{obs}}$  and  $x_p^{\text{obs}}$  distributions calculated in different kinematical regions with the ZEUS

<sup>4</sup> We use the special choice  $\mu^2 = \mathbf{k}_T^2$  in the case of the KMS gluon, as it was originally proposed in [14].

<sup>5</sup> Here and in the following all kinematic quantities are given in the laboratory frame where positive the OZ axis direction is given by the proton beam.

<sup>1</sup> lipatov@theory.sinp.msu.ru

<sup>2</sup> The most relevant properties of different unintegrated gluon distributions are discussed in [12, 13].

<sup>3</sup> See [34] for more details.

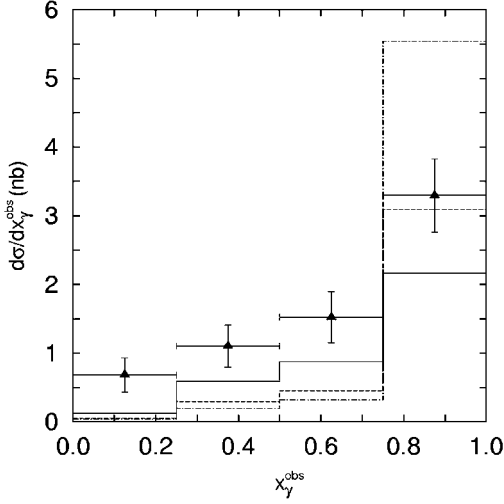


**Fig. 1.** The differential cross section  $d\sigma/dx_\gamma^{\text{obs}}$  for dijets with an associated  $D^*$  meson with  $p_T^{D^*} > 3$  GeV,  $-1.5 < \eta^{D^*} < 1.5$  in the kinematic range  $130 < W < 280$  GeV,  $Q^2 < 1$  GeV<sup>2</sup>,  $|\eta^{\text{jet}}| < 2.4$ ,  $E_T^{\text{jet}1} > 7$  GeV and  $E_T^{\text{jet}2} > 6$  GeV. The *solid*, *dashed* and *dash-dotted* histograms correspond to the J2003 (set 1), KMR and KMS unintegrated gluon distributions, respectively. The experimental data are from ZEUS [1]

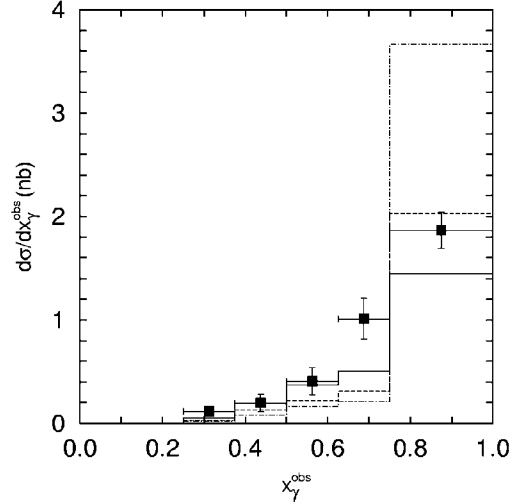


**Fig. 3.** The differential cross section  $d\sigma/dx_\gamma^{\text{obs}}$  for dijets with an associated  $D^*$  meson with  $p_T^{D^*} > 3$  GeV,  $-1.5 < \eta^{D^*} < 1.5$  in the kinematic range  $130 < W < 280$  GeV,  $Q^2 < 1$  GeV<sup>2</sup>,  $|\eta^{\text{jet}}| < 2.4$ ,  $E_T^{\text{jet}1} > 5$  GeV,  $M > 18$  GeV and  $|\bar{\eta}^{\text{jet}}| < 0.7$ . The notation of the histograms is the same as in Fig. 1. The experimental data are from ZEUS [2]

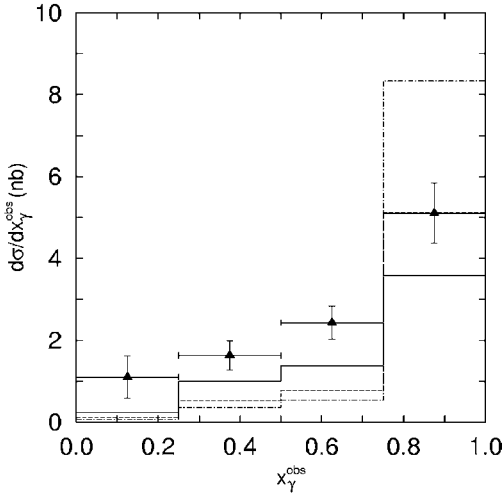


**Fig. 2.** The differential cross section  $d\sigma/dx_\gamma^{\text{obs}}$  for dijets with an associated  $D^*$  meson with  $p_T^{D^*} > 3$  GeV,  $-1.5 < \eta^{D^*} < 1.5$  in the kinematic range  $130 < W < 280$  GeV,  $Q^2 < 1$  GeV<sup>2</sup>,  $|\eta^{\text{jet}}| < 2.4$ ,  $E_T^{\text{jet}1} > 6$  GeV and  $E_T^{\text{jet}2} > 5$  GeV. The notation of the histograms is the same as in Fig. 1. The experimental data are from ZEUS [1]

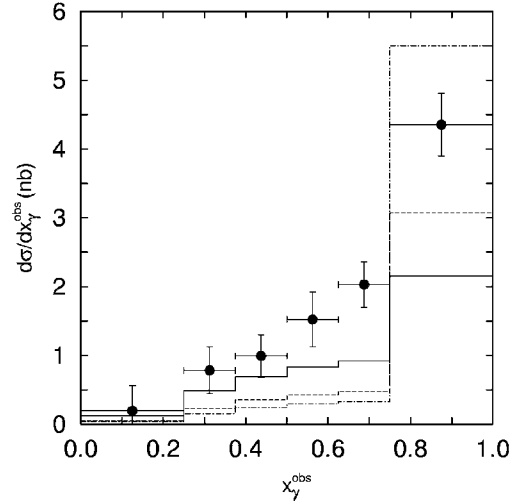


**Fig. 4.** The differential cross section  $d\sigma/dx_\gamma^{\text{obs}}$  for dijets with an associated  $D^*$  meson with  $p_T^{D^*} > 3$  GeV,  $-1.5 < \eta^{D^*} < 1.5$  in the kinematic range  $130 < W < 280$  GeV,  $Q^2 < 1$  GeV<sup>2</sup>,  $-1.5 < \eta^{\text{jet}} < 2.4$ ,  $E_T^{\text{jet}1} > 7$  GeV and  $E_T^{\text{jet}2} > 6$  GeV. The notation of the histograms the the same as in Fig. 1. The experimental data are from ZEUS [3]

data. The solid, dashed and dash-dotted histograms correspond to the results obtained with the J2003 (set 1), the KMR and the KMS unintegrated gluon densities, respectively. In agreement with the expectation for direct photon processes, the peak in the  $x_\gamma^{\text{obs}}$  distributions at high values of  $x_\gamma^{\text{obs}}$  is observed both in the data and in the theoretical calculations. However, there is also a substantial tail to small values of  $x_\gamma^{\text{obs}}$ . As it was mentioned above, the exis-

tence of this plateau in the collinear approximation of QCD usually is attributed [1–3] to the charm excitation from a resolved photon and is interpreted as a likely signature of the photon structure. In the  $k_T$ -factorization approach this plateau indicates the fact that a gluon radiated from the evolution cascade appears to be harder than charmed quarks (produced in hard parton interaction) in a significant fraction of events. Since in our calculations we have not included the resolved photon contribution explicitly

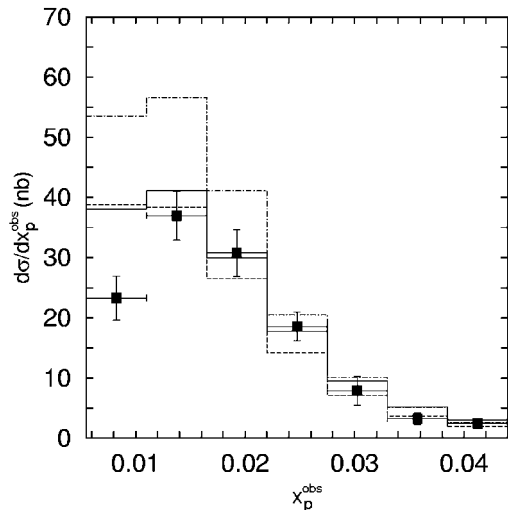


**Fig. 5.** The differential cross section  $d\sigma/dx_p^{\text{obs}}$  for dijets with an associated  $D^*$  meson with  $p_T^{D^*} > 3$  GeV,  $-1.5 < \eta^{D^*} < 1.5$  in the kinematic range  $130 < W < 280$  GeV,  $Q^2 < 1$  GeV<sup>2</sup>,  $|\eta^{\text{jets}}| < 2.4$ ,  $E_T^{\text{jets}} > 5$  GeV,  $M > 18$  GeV and  $|\eta^{\text{jets}}| < 0.7$ . The notation of the histograms is the same as in Fig. 1. The experimental data are from ZEUS [2]

and have operated in terms of the proton structure only, we can conclude that the  $k_T$ -factorization approach effectively imitates the charm component of the photon [24, 25]. However, the predicted tail at small  $x_\gamma^{\text{obs}}$  values is strongly dependent on the unintegrated gluon distributions. Our results corresponding to different gluon densities do not agree well with the ZEUS data in Figs. 1, 2 and 4. The calculated cross sections at low  $x_\gamma^{\text{obs}}$  are defined by the average value of the gluon transverse momenta  $\langle k_T \rangle$  which is generated in the course of the non-collinear evolution. It is because the events, when the gluon jet has the largest and next-to-largest  $p_T$  among the three hadron jets, contribute only in this kinematical region [24]. Therefore we can conclude that the average gluon  $\langle k_T \rangle$  generated by all three versions of the unintegrated gluon distributions under consideration is too small to describe the ZEUS data. However, Fig. 3 shows that the theoretical results obtained with the J2003 and KMR unintegrated gluon distributions well describe the experimental data with the cut on the dijet invariant mass  $M > 18$  GeV. It demonstrates that this cut is essential for the applicability of the description of resolved photon contributions by non-collinear evolution only.

We would like to note that the events with a small  $x_\gamma^{\text{obs}}$  also may originate by the components of resolved photon which contain a gluon (i.e. gluon-gluon fusion subprocess). However, the analysis [2] which was performed by the ZEUS collaboration indicates that such a contribution is very small: most of the resolved photon contribution in LO QCD charm production is due to charm originating from the photon, rather than to the competing resolved photon process  $gg \rightarrow c\bar{c}$ . We estimate such a contribution in the framework of the  $k_T$ -factorization approach using the KMR-constructed unintegrated gluon distributions in

a proton and in a photon. We find that it gives a contribution of only about 2% to the cross section at  $x_\gamma^{\text{obs}} < 0.75$  (not shown in the figures). Therefore we will not take into account gluon-gluon fusion in the following theoretical calculations<sup>6</sup>.

The collinear NLO massive calculations [20] give a similar description of the ZEUS data for  $d\sigma/x_\gamma^{\text{obs}}$ : the cross sections predicted by the NLO calculations reproduce the data in the direct photon-like region but they are below the data in the resolved photon-like one [1–3]. This fact clearly demonstrates again that the  $k_T$ -factorization approach effectively simulates charm quark excitation processes which give a main contribution to the NLO cross section at low  $x_\gamma^{\text{obs}}$ . Note also that according to the analysis [2, 3] which was done by the ZEUS collaboration, in order to obtain a realistic comparison of their data and theory the corrections for hadronization should be taken into account in the predictions<sup>7</sup>. The correction factors are typically 0.8–1.1 depending on the bin. These factors are not accounted for in our analysis.

The similar description of the data [1] was obtained in [25] where the JS unintegrated gluon density [41] and Monte Carlo generator CASCADE [28] have been applied. However, our predictions lie significantly below the results presented in [24]. The reasons of this discrepancy are connected with the parameter settings accepted in [24]. In particular, in [24] the unintegrated gluon distribution proposed by Blümlein [42] has been used.

The differential cross section as a function of  $x_p^{\text{obs}}$  is shown in Fig. 5. The shape of the  $x_p^{\text{obs}}$  distribution is well reproduced by all unintegrated gluon densities under interest. However, the KMS gluon distribution (which is successful in the description of the bottom production at Tevatron [26, 43] and deep inelastic  $J/\psi$  production at HERA [44]) significantly overestimates the data at low values of  $x_p^{\text{obs}}$ , namely  $x_p^{\text{obs}} < 0.02$ . This fact is connected with the special choice of the renormalization scale  $\mu^2 = \mathbf{k}_T^2$  in the running coupling constant. The J2003 (set 1) and KMR gluon densities are in good agreement with the data. Note that the measured cross section  $d\sigma/dx_p^{\text{obs}}$  are also well described by the massive NLO QCD predictions. However the data tend to agree better with the upper bound of these calculations.

### 3.2 Angular distributions

Figures 6 and 7 show the differential cross section as a function of  $|\cos\theta^*|$  separately for the direct-enriched ( $x_\gamma^{\text{obs}} > 0.75$ ) and resolved-enriched ( $x_\gamma^{\text{obs}} < 0.75$ ) samples. As it was mentioned above, the study of these distributions gives us the possibility to learn about the size of the contribution from different production mechanisms. This is because the angular dependence of the subprocess involving

<sup>6</sup> It was demonstrated [40] that the contribution from gluon-gluon fusion is important in the description of the recent experimental data on the beauty photoproduction at HERA.

<sup>7</sup> See [2, 3] for more details.

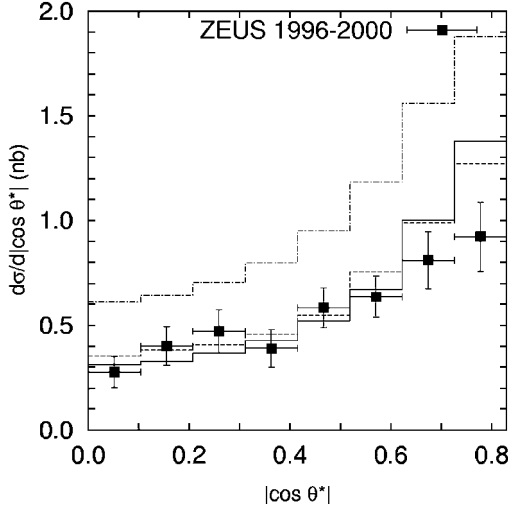


**Fig. 6.** The differential cross section  $d\sigma/d|\cos\theta^*|$  for dijets with an associated  $D^*$  meson with  $p_T^{D^*} > 3$  GeV,  $-1.5 < \eta^{D^*} < 1.5$  in the kinematic range  $130 < W < 280$  GeV,  $Q^2 < 1$  GeV<sup>2</sup>,  $|\eta^{\text{j}et}| < 2.4$ ,  $E_T^{\text{j}et} > 5$  GeV,  $M > 18$  GeV,  $|\bar{\eta}^{\text{j}et}| < 0.7$  and  $x_\gamma^{\text{obs}} > 0.75$ . The notation of the histograms is the same as in Fig. 1. The experimental data are from ZEUS [2]

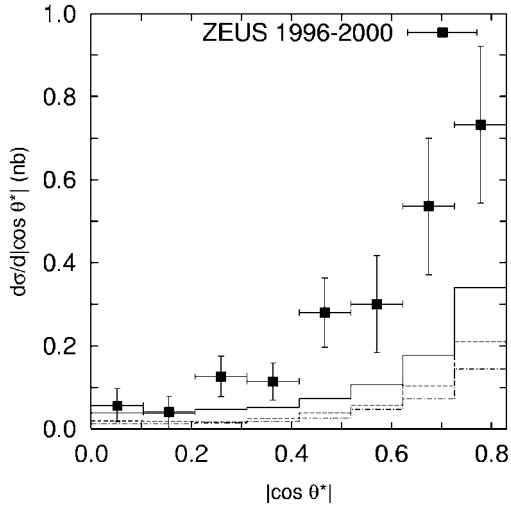


**Fig. 7.** The differential cross section  $d\sigma/d|\cos\theta^*|$  for dijets with an associated  $D^*$  meson with  $p_T^{D^*} > 3$  GeV,  $-1.5 < \eta^{D^*} < 1.5$  in the kinematic range  $130 < W < 280$  GeV,  $Q^2 < 1$  GeV<sup>2</sup>,  $|\eta^{\text{j}et}| < 2.4$ ,  $E_T^{\text{j}et} > 5$  GeV,  $M > 18$  GeV,  $|\bar{\eta}^{\text{j}et}| < 0.7$  and  $x_\gamma^{\text{obs}} < 0.75$ . The notation of the histograms is the same as in Fig. 1. The experimental data are from ZEUS [2]

a gluon propagator in the  $t$  channel is approximately proportional to  $(1 - |\cos\theta^*|)^{-2}$ , whereas it is proportional to  $(1 - |\cos\theta^*|)^{-1}$  in the case of a quark propagator. So from Fig. 6 one can see that the direct photon-like events give a slow increase in the cross section with increasing  $|\cos\theta^*|$  (in the proton direction) both in the data and in the theoretical calculations. The resolved photon-like events exhibit a more rapid rise towards high values of  $|\cos\theta^*|$  (see Fig. 7). Such a behavior is suggested by the large gluon-exchange contribution of the charm-excitation process. In

our theoretical calculations, the shape of the data is reproduced very well, but the overall normalization is rather low compared to the data. Note that the collinear NLO predictions [20] are also significantly below the data at low  $x_\gamma^{\text{obs}}$  [2].

In the further analysis [2] which was done by the ZEUS collaboration, the two jets were distinguished by associating the  $D^*$  meson to the closest jet in the  $\eta$ - $\phi$  plane. The associated jet is defined as the jet with the smallest  $R_i^2 = (\eta^{\text{j}et_i} - \eta^{D^*})^2 + (\phi^{\text{j}et_i} - \phi^{D^*})^2$ , where  $\phi^{\text{j}et_i}$  and  $\phi^{D^*}$  are the azimuthal angles of the jets and the  $D^*$  meson in the laboratory frame. Calling this ‘‘associated jet’’ jet 1 in (7), the rise of  $d\sigma/d\cos\theta^*$  can be studied [2]. Figures 8 and 9 show the differential cross sections as a function of  $\cos\theta^*$  for the direct-enriched and resolved-enriched samples. The resolved photon-like events exhibit a mild rise in the proton hemisphere towards  $\cos\theta^* = 1$ , consistent with expectations from quark exchange. In contrast, they have a strong rise towards  $\cos\theta^* = -1$ , i.e. in the photon direction, consistent with a dominant contribution from gluon exchange. In our theoretical calculations, the peak at  $\cos\theta^* = -1$  at low  $x_\gamma^{\text{obs}}$  clearly illustrates again that the  $k_T$ -factorization approach effectively reproduces the charm-excitation processes using only the photon-gluon fusion off-mass shell matrix elements. It is necessary to note that these matrix elements correspond to the  $2 \rightarrow 2$  partonic subprocess with the charm-anticharm pair in the final state and therefore is fully symmetric in  $\cos\theta^*$ . This fact leads to the symmetric  $\cos\theta^*$  distribution at high  $x_\gamma^{\text{obs}}$  (see Fig. 8). However, the angular distribution  $d\sigma/d\cos\theta^*$  exhibits a slight asymmetry in the data as well in the NLO predictions which is explained [2] by the feedthrough from the resolved photon processes near  $\cos\theta^* = -1$ . So we can conclude that all three unintegrated gluon densi-

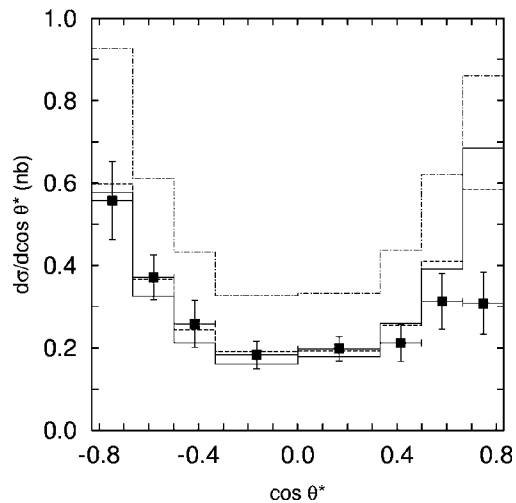


**Fig. 8.** The differential cross section  $d\sigma/d\cos\theta^*$  for dijets with an associated  $D^*$  meson with  $p_T^{D^*} > 3$  GeV,  $-1.5 < \eta^{D^*} < 1.5$  in the kinematic range  $130 < W < 280$  GeV,  $Q^2 < 1$  GeV<sup>2</sup>,  $|\eta^{\text{j}et}| < 2.4$ ,  $E_T^{\text{j}et} > 5$  GeV,  $M > 18$  GeV,  $|\bar{\eta}^{\text{j}et}| < 0.7$  and  $x_\gamma^{\text{obs}} > 0.75$ . The notation of the histograms is the same as in Fig. 1. The experimental data are from ZEUS [2]

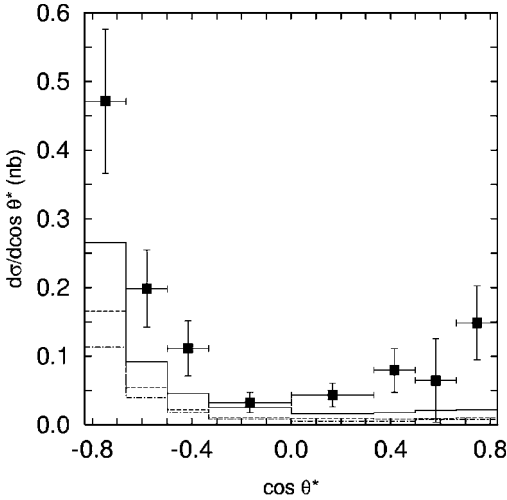


**Fig. 9.** The differential cross section  $d\sigma/d \cos \theta^*$  for dijets with an associated  $D^*$  meson with  $p_T^{D^*} > 3$  GeV,  $-1.5 < \eta^{D^*} < 1.5$  in the kinematic range  $130 < W < 280$  GeV,  $Q^2 < 1$  GeV<sup>2</sup>,  $|\eta^{\text{jet}}| < 2.4$ ,  $E_T^{\text{jet}} > 5$  GeV,  $M > 18$  GeV,  $|\bar{\eta}^{\text{jet}}| < 0.7$  and  $x_\gamma^{\text{obs}} < 0.75$ . The notation of the histograms is the same as in Fig. 1. The experimental data are from ZEUS [2]

ties studied here overestimate the data at high values of  $\cos \theta^*$  and  $x_\gamma^{\text{obs}}$ .

### 3.3 The invariant mass distributions and azimuthal correlations

Very recently the ZEUS collaboration has measured [3] the cross sections of the  $D^*$  meson and associated dijet production as a function of the dijet invariant mass  $M$ , and the correlations between the final hadronic jets, namely

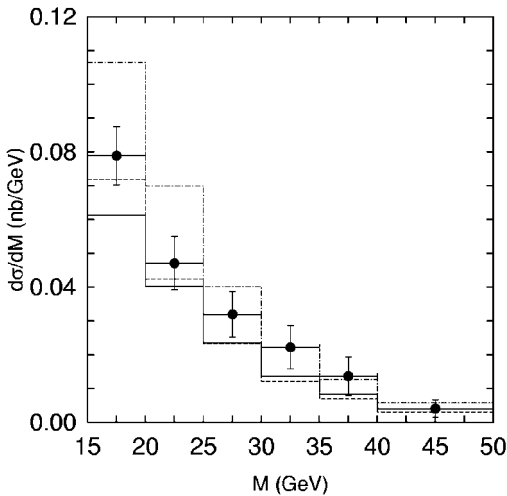


**Fig. 10.** The differential cross section  $d\sigma/dM$  for dijets with an associated  $D^*$  meson with  $p_T^{D^*} > 3$  GeV,  $-1.5 < \eta^{D^*} < 1.5$  in the kinematic range  $130 < W < 280$  GeV,  $Q^2 < 1$  GeV<sup>2</sup>,  $-1.5 < \eta^{\text{jet}} < 2.4$ ,  $E_T^{\text{jet}_1} > 7$  GeV,  $E_T^{\text{jet}_2} > 6$  GeV and  $x_\gamma^{\text{obs}} > 0.75$ . The notation of the histograms is the same as in Fig. 1. The experimental data are from ZEUS [3]

the difference in azimuthal angle  $\Delta\phi = |\phi^{\text{jet}_1} - \phi^{\text{jet}_2}|$ , and the transverse momentum  $p_T$  distributions of the dijet system ( $\mathbf{p}_T = \mathbf{p}_T^{\text{jet}_1} + \mathbf{p}_T^{\text{jet}_2}$ ). As it was mentioned above, the  $\Delta\phi$  and  $p_T$  distributions are particularly sensitive to higher-order corrections and to the unintegrated gluon densities in the proton. In Figs. 10–18 the differential dijet cross sections as a function of these variables are shown in different  $x_\gamma^{\text{obs}}$  regions. We see again that the agreement between the theoretical calculations and the data is better

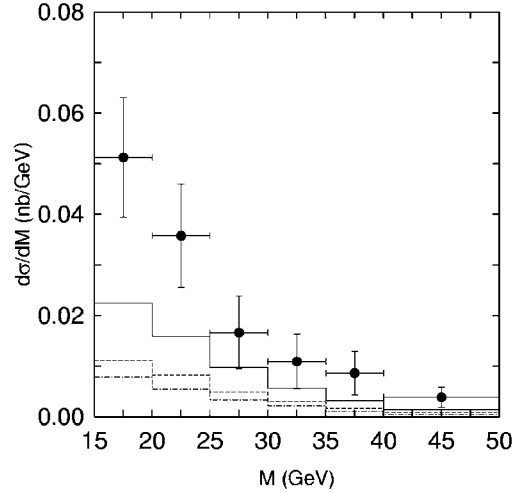


**Fig. 11.** The differential cross section  $d\sigma/dM$  for dijets with an associated  $D^*$  meson with  $p_T^{D^*} > 3$  GeV,  $-1.5 < \eta^{D^*} < 1.5$  in the kinematic range  $130 < W < 280$  GeV,  $Q^2 < 1$  GeV<sup>2</sup>,  $-1.5 < \eta^{\text{jet}} < 2.4$ ,  $E_T^{\text{jet}_1} > 7$  GeV,  $E_T^{\text{jet}_2} > 6$  GeV and  $x_\gamma^{\text{obs}} < 0.75$ . The notation of the histograms is the same as in Fig. 1. The experimental data are from ZEUS [3]

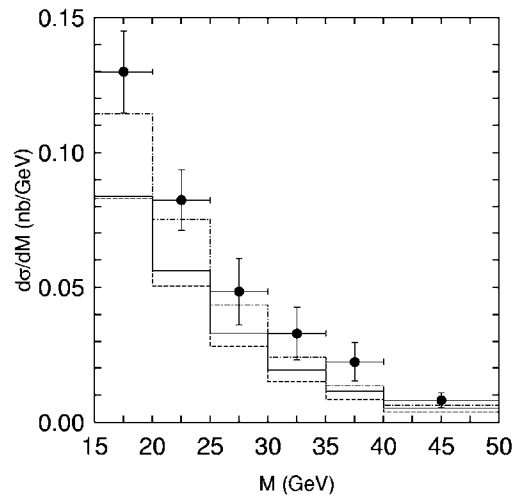


**Fig. 12.** The differential cross section  $d\sigma/dM$  for dijets with an associated  $D^*$  meson with  $p_T^{D^*} > 3$  GeV,  $-1.5 < \eta^{D^*} < 1.5$  in the kinematic range  $130 < W < 280$  GeV,  $Q^2 < 1$  GeV<sup>2</sup>,  $-1.5 < \eta^{\text{jet}} < 2.4$ ,  $E_T^{\text{jet}_1} > 7$  GeV and  $E_T^{\text{jet}_2} > 6$  GeV. The notation of the histograms is the same as in Fig. 1. The experimental data are from ZEUS [3]



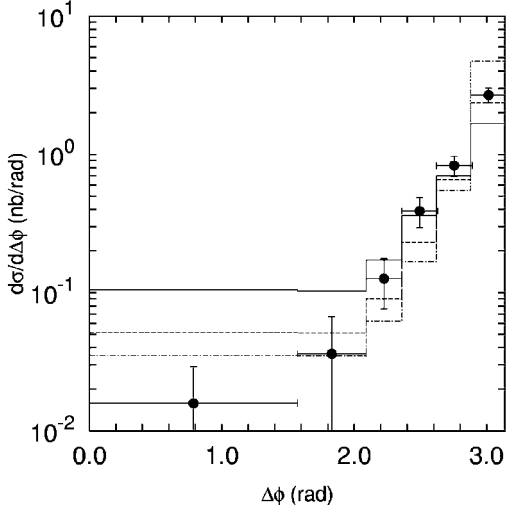


**Fig. 13.** The differential cross section  $d\sigma/d\Delta\phi$  for dijets with an associated  $D^*$  meson with  $p_T^{D^*} > 3$  GeV,  $-1.5 < \eta^{D^*} < 1.5$  in the kinematic range  $130 < W < 280$  GeV,  $Q^2 < 1$  GeV<sup>2</sup>,  $-1.5 < \eta^{\text{jet}} < 2.4$ ,  $E_T^{\text{jet}1} > 7$  GeV,  $E_T^{\text{jet}2} > 6$  GeV and  $x_\gamma^{\text{obs}} > 0.75$ . The notation of the histograms is the same as in Fig. 1. The experimental data are from ZEUS [3]

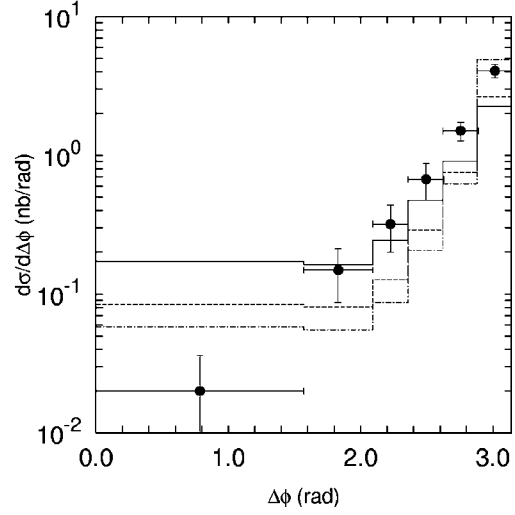


**Fig. 15.** The differential cross section  $d\sigma/d\Delta\phi$  for dijets with an associated  $D^*$  meson with  $p_T^{D^*} > 3$  GeV,  $-1.5 < \eta^{D^*} < 1.5$  in the kinematic range  $130 < W < 280$  GeV,  $Q^2 < 1$  GeV<sup>2</sup>,  $-1.5 < \eta^{\text{jet}} < 2.4$ ,  $E_T^{\text{jet}1} > 7$  GeV and  $E_T^{\text{jet}2} > 6$  GeV. The notation of the histograms is the same as in Fig. 1. The experimental data are from ZEUS [3]

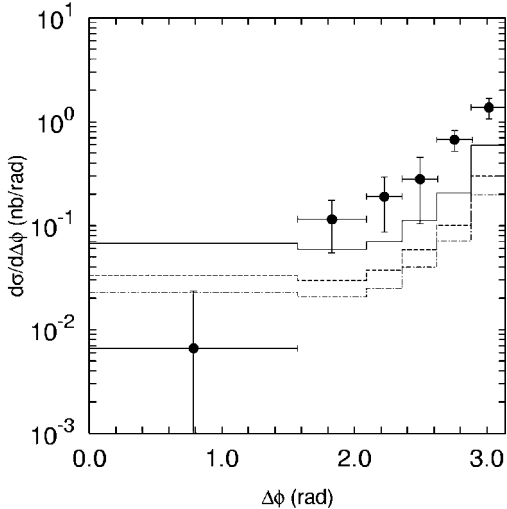


**Fig. 14.** The differential cross section  $d\sigma/d\Delta\phi$  for dijets with an associated  $D^*$  meson with  $p_T^{D^*} > 3$  GeV,  $-1.5 < \eta^{D^*} < 1.5$  in the kinematic range  $130 < W < 280$  GeV,  $Q^2 < 1$  GeV<sup>2</sup>,  $-1.5 < \eta^{\text{jet}} < 2.4$ ,  $E_T^{\text{jet}1} > 7$  GeV,  $E_T^{\text{jet}2} > 6$  GeV and  $x_\gamma^{\text{obs}} < 0.75$ . The notation of the histograms is the same as in Fig. 1. The experimental data are from ZEUS [3]

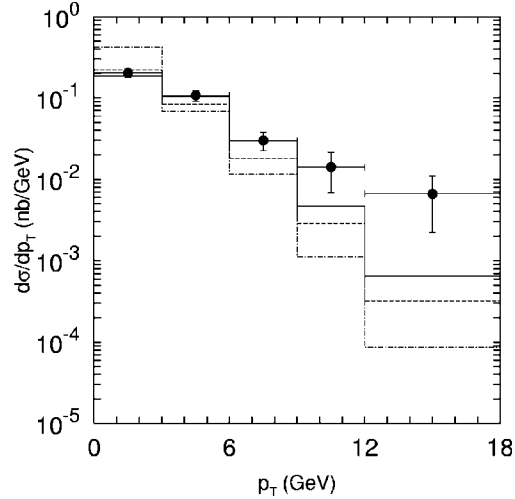


**Fig. 16.** The differential cross section  $d\sigma/dp_T$  for dijets with an associated  $D^*$  meson with  $p_T^{D^*} > 3$  GeV,  $-1.5 < \eta^{D^*} < 1.5$  in the kinematic range  $130 < W < 280$  GeV,  $Q^2 < 1$  GeV<sup>2</sup>,  $-1.5 < \eta^{\text{jet}} < 2.4$ ,  $E_T^{\text{jet}1} > 7$  GeV,  $E_T^{\text{jet}2} > 6$  GeV and  $x_\gamma^{\text{obs}} > 0.75$ . The notation of the histograms is the same as in Fig. 1. The experimental data are from ZEUS [3]

for the direct-enriched events in comparison with resolved-enriched ones. In spite of the fact that all histograms in Figs. 13–15 lie above the data at  $\Delta\phi \sim 0$ , the shape of the  $\Delta\phi$  distribution at  $x_\gamma^{\text{obs}} > 0.75$  strongly depends on the unintegrated gluon densities used. The J2003 density gives a significantly harder distribution compared to the data whereas the KMS one gives a softer distribution. In contrast, in the low  $x_\gamma^{\text{obs}}$  region the shapes of the  $\Delta\phi$  spectrum predicted by the different gluon distributions

are very similar to each other. Therefore by analogy with the bottom production at Tevatron [26] we can conclude that the properties of different unintegrated gluon densities manifest themselves in the dijet azimuthal correlations at high values of  $x_\gamma^{\text{obs}}$ . Concerning the  $p_T$ -spectra, we see in Figs. 16–18 that our predictions have a significantly softer  $p_T$  distribution at large  $p_T$  compared to the data for both direct and resolved photon events. In fact, a reasonable agreement with the ZEUS data in the restricted  $p_T$  region ( $p_T < 10$  GeV) can be obtained using the J2003 (set 1)

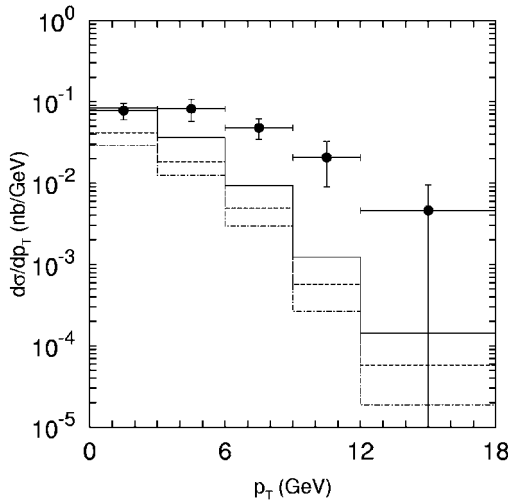


**Fig. 17.** The differential cross section  $d\sigma/dp_T$  for dijets with an associated  $D^*$  meson with  $p_T^{D^*} > 3$  GeV,  $-1.5 < \eta^{D^*} < 1.5$  in the kinematic range  $130 < W < 280$  GeV,  $Q^2 < 1$  GeV<sup>2</sup>,  $-1.5 < \eta^{\text{j}et} < 2.4$ ,  $E_T^{\text{j}et_1} > 7$  GeV,  $E_T^{\text{j}et_2} > 6$  GeV and  $x_\gamma^{\text{obs}} < 0.75$ . The notation of the histograms is the same as in Fig. 1. The experimental data are from ZEUS [3]

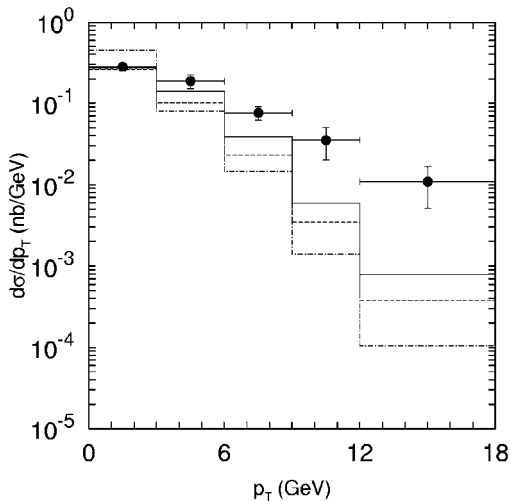


**Fig. 18.** The differential cross section  $d\sigma/dp_T$  for dijets with an associated  $D^*$  meson with  $p_T^{D^*} > 3$  GeV,  $-1.5 < \eta^{D^*} < 1.5$  in the kinematic range  $130 < W < 280$  GeV,  $Q^2 < 1$  GeV<sup>2</sup>,  $-1.5 < \eta^{\text{j}et} < 2.4$ ,  $E_T^{\text{j}et_1} > 7$  GeV and  $E_T^{\text{j}et_2} > 6$  GeV. The notation of the histograms is the same as in Fig. 1. The experimental data are from ZEUS [3]

gluon only. The shape of this distribution is also very different for different unintegrated gluon densities. The KMS gluon distribution gives the very soft  $p_T$  spectrum in comparison with the J2003 and KMR densities and significantly (by a factor about 3) overestimate the data at low  $p_T$  (except in the small  $x_\gamma^{\text{obs}}$  region). The collinear NLO predictions [20] at high  $x_\gamma^{\text{obs}}$  also show a large deviation from the measured cross sections  $d\sigma/d\Delta\phi$  and  $d\sigma/dp_T$  at low  $\Delta\phi$  and high  $p_T$  [3]. This discrepancy is essentially

enhanced to the resolved-enriched events. Since the small  $x_\gamma^{\text{obs}}$  region is expected to be particularly sensitive to high-order corrections, further theoretical attempts to reduce the observed discrepancy are necessary.

Finally, we can conclude that the results presented here clearly demonstrate that agreement between the theoretical calculations and recent ZEUS data for charm production at HERA is far from ideal and for many observables coincide with the NLO results. We have obtained a rather good description of the HERA data with the J2003 (set 1) and KMR unintegrated gluon distributions in direct photon-like region, but faulty description for many observables in the resolved photon-like photon region. In the framework of the  $k_T$ -factorization, the different unintegrated gluon densities exhibit significantly different effects at HERA energies. This fact indicates the need for better experimental constraints as well as further theoretical studies for a more detailed understanding of the parton evolution at high energies and, in particular, for the precise description of charm with associated jets photoproduction at HERA.

## 4 Conclusions

We presented the calculations of the charm and dijet associated photoproduction at HERA energies in the  $k_T$ -factorization approach. We used the unintegrated gluon densities in a proton which are obtained from the full CCFM, from the unified BFKL-DGLAP evolution equations as well as from the Kimber–Martin–Ryskin prescription. The ability of these  $k_T$ -dependent gluon densities to reproduce the recent experimental data taken by the ZEUS collaboration has been investigated. The calculations of the number of dijet correlations in the framework of the  $k_T$ -factorization were performed for the first time.

Our investigations were based on the leading-order off-mass shell matrix elements for the photon–gluon fusion subprocess. We have shown that these matrix elements combined with the non-collinear evolution of gluon densities in a proton effectively simulate the charmed quark excitation processes and indeed the hardest  $p_T$  emission comes frequently from a gluon in the initial-state gluon cascade<sup>8</sup>. We demonstrated that the wide plateau seen in the  $x_\gamma^{\text{obs}}$  distributions (usually attributed to the charm excitation from a resolved photon) is connected with the average value of the gluon transverse momenta  $\langle k_T \rangle$  which is generated in the course of the non-collinear evolution. Special attention has been given to the specific angular correlations between the hadronic jets in the final state. We find that the properties of different unintegrated gluon densities manifest themselves in the dijet azimuthal correlations at high  $x_\gamma^{\text{obs}}$ .

The absolute cross sections predicted by the  $k_T$ -factorization calculation supplemented with the J2003 (set 1) and KMR unintegrated gluon distributions reproduce the

<sup>8</sup> In this part our conclusions coincide with the ones from [24, 25].

numerous HERA data for the sample enriched in direct photons but are below the data for the sample enriched in resolved photons. Therefore further theoretical studies for a more detailed understanding of parton evolution in a proton in the small- $x$  region are necessary in order to describe the charm with associated dijet photoproduction at HERA.

*Acknowledgements.* The authors are very grateful to S.P. Baranov for encouraging interest and helpful discussions, H. Jung for reading of the manuscript and very useful remarks, P.F. Ermolov for support and DESY Directorate for hospitality and support. This research was supported in part by the FASI of Russian Federation (grant NS-1685.2003.2). A.L. was supported in part by the grant of President of Russian Federation (MK-9820.2006.2).

## References

1. ZEUS Collaboration, J. Breitweg et al., *Eur. Phys. J. C* **6**, 67 (1999)
2. ZEUS Collaboration, S. Chekanov et al., *Phys. Lett. B* **565**, 87 (2003)
3. ZEUS Collaboration, S. Chekanov et al., *Nucl. Phys. B* **729**, 492 (2005)
4. H1 Collaboration, A. Aktas et al., *Eur. Phys. J. C* **41**, 453 (2005)
5. H1 Collaboration, A. Aktas et al., *Phys. Lett. B* **621**, 56 (2005)
6. V.N. Gribov, L.N. Lipatov, *Yad. Fiz.* **15**, 781 (1972); L.N. Lipatov, *Sov. J. Nucl. Phys.* **20**, 94 (1975); G. Altarelli, G. Parisi, *Nucl. Phys. B* **126**, 298 (1977); Y.L. Dokshitzer, *Sov. Phys. JETP* **46**, 641 (1977)
7. L.V. Gribov, E.M. Levin, M.G. Ryskin, *Phys. Rep.* **100**, 1 (1983)
8. E.M. Levin, M.G. Ryskin, Y.M. Shabelsky, A.G. Shuvaev, *Sov. J. Nucl. Phys.* **53**, 657 (1991)
9. S. Catani, M. Ciafaloni, F. Hautmann, *Nucl. Phys. B* **366**, 135 (1991)
10. J.C. Collins, R.K. Ellis, *Nucl. Phys. B* **360**, 3 (1991)
11. E.A. Kuraev, L.N. Lipatov, V.S. Fadin, *Sov. Phys. JETP* **44**, 443 (1976); E.A. Kuraev, L.N. Lipatov, V.S. Fadin, *Sov. Phys. JETP* **45**, 199 (1977); I.I. Balitsky, L.N. Lipatov, *Sov. J. Nucl. Phys.* **28**, 822 (1978)
12. Small- $x$  Collaboration, B. Andersson et al., *Eur. Phys. J. C* **25**, 77 (2002)
13. Small- $x$  Collaboration, J. Andersen et al., *Eur. Phys. J. C* **35**, 67 (2004)
14. J. Kwiecinski, A.D. Martin, A.M. Stasto, *Phys. Rev. D* **56**, 3991 (1997)
15. M. Ciafaloni, *Nucl. Phys. B* **296**, 49 (1988); S. Catani, F. Fiorani, G. Marchesini, *Phys. Lett. B* **234**, 339 (1990); S. Catani, F. Fiorani, G. Marchesini, *Nucl. Phys. B* **336**, 18 (1990); G. Marchesini, *Nucl. Phys. B* **445**, 49 (1995)
16. J.R. Forshaw, A. Sabio Vera, *Phys. Lett. B* **440**, 141 (1998)
17. B.R. Webber, *Phys. Lett. B* **444**, 81 (1998)
18. G.P. Salam, *JHEP* **03**, 009 (1999)
19. M.A. Kimber, A.D. Martin, M.G. Ryskin, *Phys. Rev. D* **63**, 114027 (2001); G. Watt, A.D. Martin, M.G. Ryskin, *Eur. Phys. J. C* **31**, 73 (2003)
20. S. Frixione et al., *Phys. Lett. B* **348**, 633 (1995); S. Frixione et al., *Nucl. Phys. B* **454**, 3 (1995)
21. J. Binnewies, B.A. Kniehl, G. Kramer, *Z. Phys. C* **76**, 677 (1997); M. Cacciari, M. Greco, *Phys. Rev. D* **55**, 7134 (1997); B.A. Kniehl, G. Kramer, M. Spira, *Z. Phys. C* **76**, 689 (1997)
22. J. Binnewies, B.A. Kniehl, G. Kramer, *Phys. Rev. D* **58**, 014014 (1998)
23. G. Heinrich, B.A. Kniehl, *Phys. Rev. D* **70**, 094035 (2004)
24. S.P. Baranov, N.P. Zotov, *Phys. Lett. B* **491**, 111 (2000)
25. S.P. Baranov, H. Jung, L. Jönsson, S. Padhi, N.P. Zotov, *Eur. Phys. J. C* **24**, 425 (2002)
26. S.P. Baranov, N.P. Zotov, A.V. Lipatov, *Phys. Atom. Nucl.* **67**, 834 (2004)
27. S.P. Baranov, H. Jung, L. Jönsson et al., in: *Proceedings of the XXXII Inter. Symposium on Multiparticle Dynamics*, World Scientific, Singapore, p. 195; hep-ph/03011017
28. H. Jung, *Comput. Phys. Comm.* **143**, 100 (2002)
29. A.V. Lipatov, N.P. Zotov, *Eur. Phys. J. C* **41**, 163 (2005)
30. G.P. Lepage, *J. Comput. Phys.* **27**, 192 (1978)
31. C. Peterson, D. Schlatter, I. Schmitt, P. Zerwas, *Phys. Rev. D* **27**, 105 (1983)
32. P. Nason, C. Oleari, *Nucl. Phys. B* **565**, 245 (2000)
33. OPAL Collaboration, K. Ackerstaff et al., *Eur. Phys. J. C* **1**, 439 (1998)
34. H. Jung, *Mod. Phys. Lett. A* **19**, 1 (2004)
35. J. Kwiecinski, A.D. Martin, A. Sutton, *Phys. Rev. D* **52**, 1445 (1995)
36. J. Kwiecinski, A.D. Martin, J. Outhwaite, *Eur. Phys. J. C* **9**, 611 (2001)
37. A.V. Lipatov, to be published in *Yad. Fiz.* (2006)
38. A.V. Lipatov, N.P. Zotov, *Phys. Rev. D* **72**, 054002 (2005)
39. A.V. Lipatov, N.P. Zotov, *Phys. Rev. D* **73**, 114018 (2006)
40. A.V. Lipatov, N.P. Zotov, hep-ph/0601240
41. H. Jung, G. Salam, *Eur. Phys. J. C* **19**, 351 (2001)
42. J. Blümlein, DESY 95-121
43. P. Hägler, R. Kirschner, A. Schäfer, L. Szymanowski, O.V. Teryaev, *Phys. Rev. D* **62**, 071502 (2000)
44. A.V. Lipatov, N.P. Zotov, *Eur. Phys. J. C* **27**, 87 (2003)